Today's outline - October 21, 2024

Today's outline - October 21, 2024

- Pair distribution function

Today's outline - October 21, 2024

- Pair distribution function
- Bragg & Laue geometries

Today's outline - October 21, 2024

- Pair distribution function
- Bragg & Laue geometries
- Kinematical intensity

Today's outline - October 21, 2024

- Pair distribution function
- Bragg & Laue geometries
- Kinematical intensity
- Reflection for a single layer

Today's outline - October 21, 2024

- Pair distribution function
- Bragg & Laue geometries
- Kinematical intensity
- Reflection for a single layer

Reading Assignment: Chapter 6.3-6.4

Today's outline - October 21, 2024

- Pair distribution function
- Bragg & Laue geometries
- Kinematical intensity
- Reflection for a single layer

Reading Assignment: Chapter 6.3-6.4

Homework Assignment #05:
Chapter 5: 1,2,7,9,10
due Monday, October 28, 2024

Today's outline - October 21, 2024

- Pair distribution function
- Bragg & Laue geometries
- Kinematical intensity
- Reflection for a single layer

Reading Assignment: Chapter 6.3-6.4

Homework Assignment #05:
Chapter 5: 1,2,7,9,10
due Monday, October 28, 2024

Homework Assignment #06:
Chapter 6: 1,6,7,8,9
due Monday, November 11, 2024

CaO-CO_2 reaction kinetics

CaO is a possible material to be used for carbon sequestration

A. Biasin, C.U. Segre, G. Salviulo, F. Zorzi, and M. Strumendo, *Chemical Eng. Sci.* **127**, 13-24 (2015)

CaO-CO_2 reaction kinetics

CaO is a possible material to be used for carbon sequestration

CaO will absorb CO_2 at temperatures as low as 450°C forming $CaCO_3$ and can be regenerated by calcination at temperatures above 700°C

A. Biasin, C.U. Segre, G. Salviulo, F. Zorzi, and M. Strumendo, *Chemical Eng. Sci.* **127**, 13-24 (2015)

CaO-CO_2 reaction kinetics

CaO is a possible material to be used for carbon sequestration

CaO will absorb CO_2 at temperatures as low as 450°C forming $CaCO_3$ and can be regenerated by calcination at temperatures above 700°C

It is important to understand the fundamental reaction kinetics of thse processes in order to be able to design carbon sequestration procedures.

A. Biasin, C.U. Segre, G. Salviulo, F. Zorzi, and M. Strumendo, *Chemical Eng. Sci.* **127**, 13-24 (2015)

CaO-CO_2 reaction kinetics

CaO is a possible material to be used for carbon sequestration

CaO will absorb CO_2 at temperatures as low as 450°C forming $CaCO_3$ and can be regenerated by calcination at temperatures above 700°C

It is important to understand the fundamental reaction kinetics of thse processes in order to be able to design carbon sequestration procedures.

Measurements heretofore have been performed in TGA systems which have fundamental mass flow limitations. These experiments were performed at Sector 17-BM of the APS. Samples were loaded in quartz capillaries and a 2D area detector was used to take snaps at up to 0.25s/frame.

A. Biasin, C.U. Segre, G. Salviulo, F. Zorzi, and M. Strumendo, *Chemical Eng. Sci.* **127**, 13-24 (2015)

CaO-CO_2 reaction kinetics

CaO is a possible material to be used for carbon sequestration

CaO will absorb CO_2 at temperatures as low as 450°C forming $CaCO_3$ and can be regenerated by calcination at temperatures above 700°C

It is important to understand the fundamental reaction kinetics of thse processes in order to be able to design carbon sequestration procedures.

Measurements heretofore have been performed in TGA systems which have fundamental mass flow limitations. These experiments were performed at Sector 17-BM of the APS. Samples were loaded in quartz capillaries and a 2D area detector was used to take snaps at up to 0.25s/frame.

Rietveld refinement was used to measure the lattice parameters, crystallite sizes and phase fractions during carbonation and calcination cycles

A. Biasin, C.U. Segre, G. Salviulo, F. Zorzi, and M. Strumendo, *Chemical Eng. Sci.* **127**, 13-24 (2015)

Typical diffraction pattern

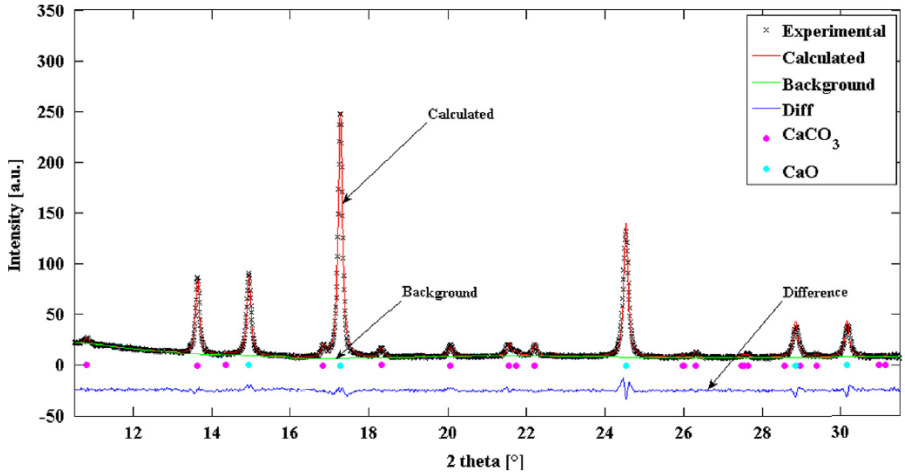

A. Biasin, C.U. Segre, G. Salviulo, F. Zorzi, and M. Strumendo, *Chemical Eng. Sci.* **127**, 13-24 (2015)

Final conversion fraction

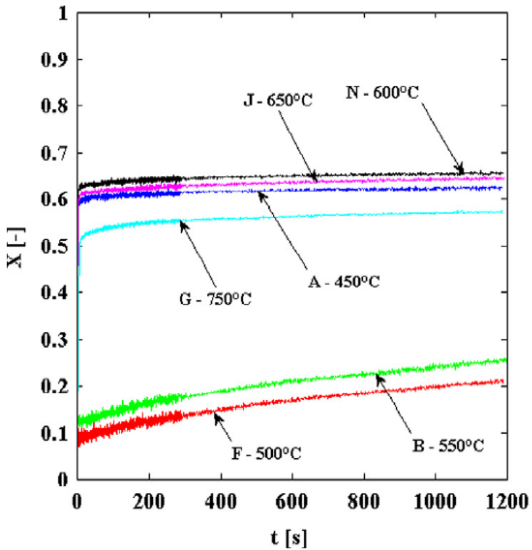

A. Biasin, C.U. Segre, G. Salviulo, F. Zorzi, and M. Strumendo, *Chemical Eng. Sci.* **127**, 13-24 (2015)

Final conversion fraction

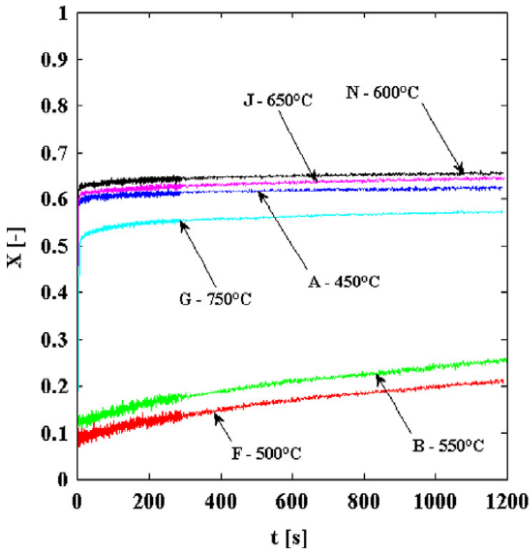

Final conversion fraction depends on temperature but also some other parameter (what?)

A. Biasin, C.U. Segre, G. Salviulo, F. Zorzi, and M. Strumendo, *Chemical Eng. Sci.* **127**, 13-24 (2015)

Final conversion fraction

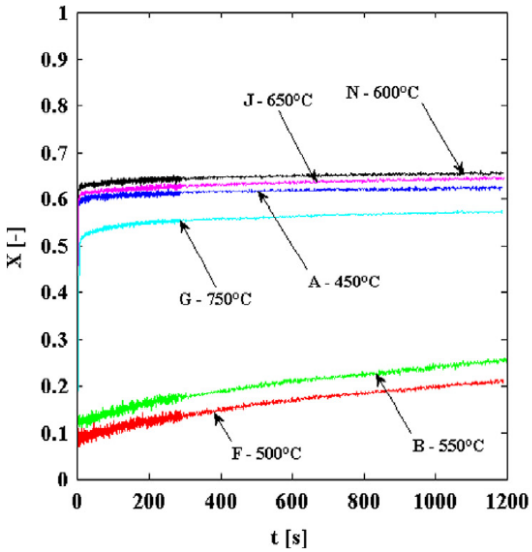

Final conversion fraction depends on temperature but also some other parameter (what?)

Remember that these powders have only been seived to a particular grain size, what about the internal structure?

A. Biasin, C.U. Segre, G. Salviulo, F. Zorzi, and M. Strumendo, *Chemical Eng. Sci.* **127**, 13-24 (2015)

$CaO\text{-}CO_2$ reaction kinetics

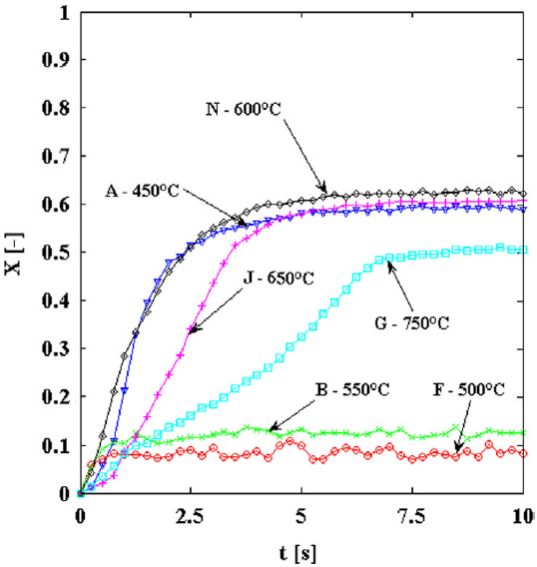

A. Biasin, C.U. Segre, G. Salviulo, F. Zorzi, and M. Strumendo, *Chemical Eng. Sci.* **127**, 13-24 (2015)

$CaO\text{-}CO_2$ reaction kinetics

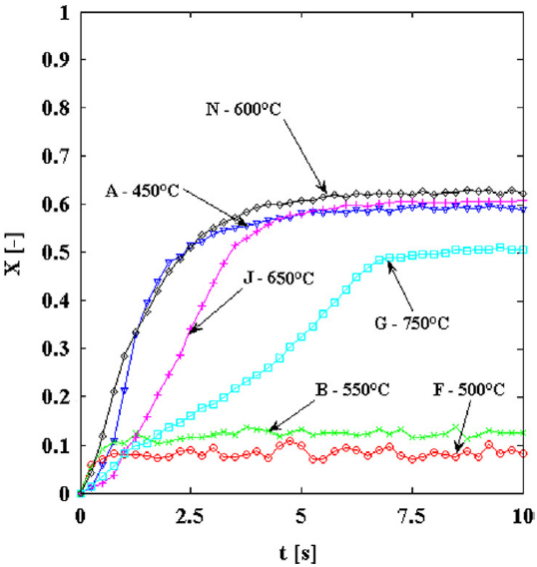

Because of the high speed of the 2D detector, it is possible to look at the conversion reaction at unprecedented time scales

A. Biasin, C.U. Segre, G. Salviulo, F. Zorzi, and M. Strumendo, *Chemical Eng. Sci.* **127**, 13-24 (2015)

$CaO\text{-}CO_2$ reaction kinetics

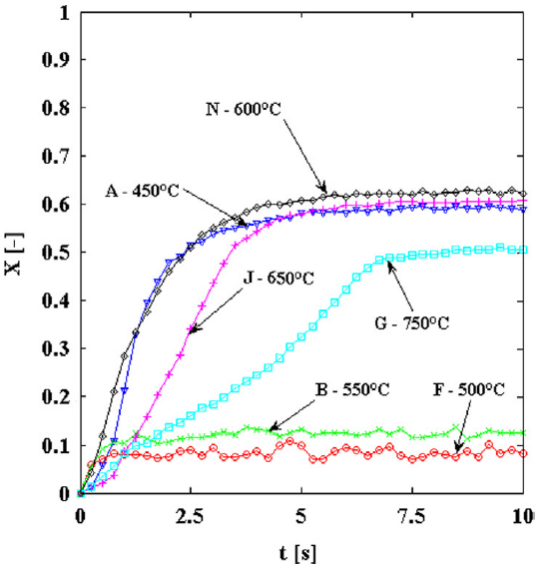

Because of the high speed of the 2D detector, it is possible to look at the conversion reaction at unprecedented time scales

Reaction kinetics much faster, $1/\tau = 0.28\ s^{-1}$, than previously observed with TGA measurements

A. Biasin, C.U. Segre, G. Salviulo, F. Zorzi, and M. Strumendo, *Chemical Eng. Sci.* **127**, 13-24 (2015)

CaO-CO_2 reaction kinetics

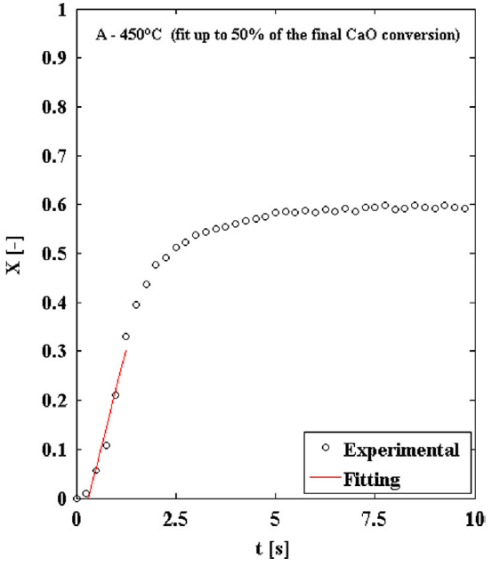

A. Biasin, C.U. Segre, G. Salviulo, F. Zorzi, and M. Strumendo, *Chemical Eng. Sci.* **127**, 13-24 (2015)

$CaO\text{-}CO_2$ reaction kinetics

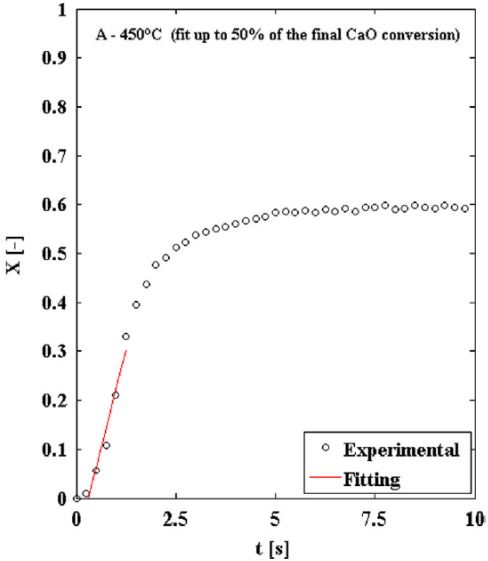

The rates of conversion are determined by fitting the initial (up to 50%) slope of the phase fraction as a function of time with a straight line

A. Biasin, C.U. Segre, G. Salviulo, F. Zorzi, and M. Strumendo, *Chemical Eng. Sci.* **127**, 13-24 (2015)

$CaO\text{-}CO_2$ reaction kinetics

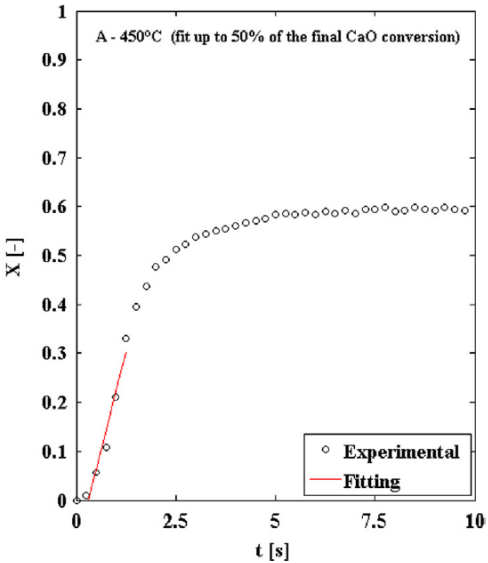

The rates of conversion are determined by fitting the initial (up to 50%) slope of the phase fraction as a function of time with a straight line

These data are then plotted versus the initial CaO crystallite size as determined by Rietveld refinements

A. Biasin, C.U. Segre, G. Salviulo, F. Zorzi, and M. Strumendo, *Chemical Eng. Sci.* **127**, 13-24 (2015)

CaO-CO_2 reaction kinetics

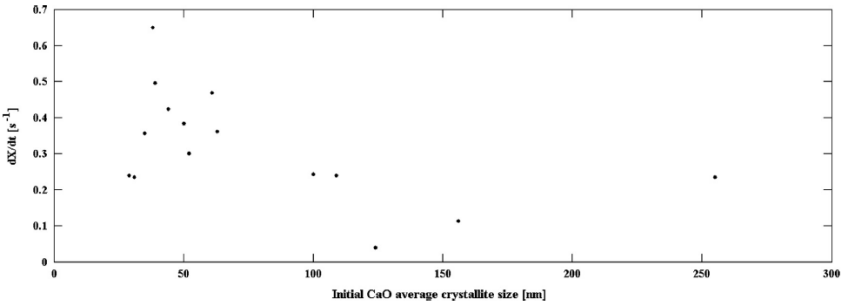

Initial crystallite size is one of the determining factors in inital rate of conversion and fraction converted.

A. Biasin, C.U. Segre, G. Salviulo, F. Zorzi, and M. Strumendo, *Chemical Eng. Sci.* **127**, 13-24 (2015)

CaO-CO_2 reaction kinetics

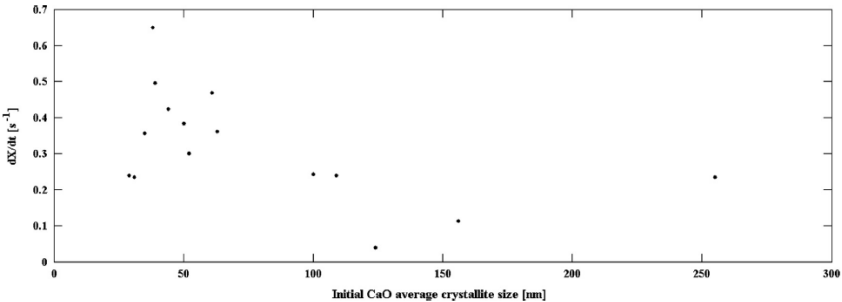

Initial crystallite size is one of the determining factors in inital rate of conversion and fraction converted.

CaO crystallite size can be related to porosity which is key to the conversion process.

A. Biasin, C.U. Segre, G. Salviulo, F. Zorzi, and M. Strumendo, *Chemical Eng. Sci.* **127**, 13-24 (2015)

Pair distribution function

By treating powder diffraction patterns using total scattering methods it is possible to study disorder in crystalline materials as well as nanocrystalline materials

Pair distribution function

By treating powder diffraction patterns using total scattering methods it is possible to study disorder in crystalline materials as well as nanocrystalline materials

The theoretical approach is identical to that for short range order and SAXS, starting with the total scattered intensity from a multi-atomic system

Pair distribution function

By treating powder diffraction patterns using total scattering methods it is possible to study disorder in crystalline materials as well as nanocrystalline materials

The theoretical approach is identical to that for short range order and SAXS, starting with the total scattered intensity from a multi-atomic system

$$I(\vec{Q}) = \sum_n f_n(\vec{Q}) e^{i\vec{Q}\cdot\vec{r_n}} \sum_m f_m^*(\vec{Q}) e^{-i\vec{Q}\cdot\vec{r_m}}$$

Pair distribution function

By treating powder diffraction patterns using total scattering methods it is possible to study disorder in crystalline materials as well as nanocrystalline materials

The theoretical approach is identical to that for short range order and SAXS, starting with the total scattered intensity from a multi-atomic system

$$I(\vec{Q}) = \sum_n f_n(\vec{Q}) e^{i\vec{Q}\cdot\vec{r_n}} \sum_m f_m^*(\vec{Q}) e^{-i\vec{Q}\cdot\vec{r_m}} = \sum_{n,m} f_n(\vec{Q}) f_m^*(\vec{Q}) e^{i\vec{Q}\cdot(\vec{r_n}-\vec{r_m})}$$

Pair distribution function

By treating powder diffraction patterns using total scattering methods it is possible to study disorder in crystalline materials as well as nanocrystalline materials

The theoretical approach is identical to that for short range order and SAXS, starting with the total scattered intensity from a multi-atomic system

$$I(\vec{Q}) = \sum_n f_n(\vec{Q}) e^{i\vec{Q}\cdot\vec{r_n}} \sum_m f_m^*(\vec{Q}) e^{-i\vec{Q}\cdot\vec{r_m}} = \sum_{n,m} f_n(\vec{Q}) f_m^*(\vec{Q}) e^{i\vec{Q}\cdot(\vec{r_n}-\vec{r_m})}$$
$$= N\langle f(\vec{Q})^2\rangle + \sum_{n,m\neq n} f_m(\vec{Q}) f_n^*(\vec{Q}) e^{i\vec{Q}\cdot(\vec{r_n}-\vec{r_m})}$$

Pair distribution function

By treating powder diffraction patterns using total scattering methods it is possible to study disorder in crystalline materials as well as nanocrystalline materials

The theoretical approach is identical to that for short range order and SAXS, starting with the total scattered intensity from a multi-atomic system

$$I(\vec{Q}) = \sum_n f_n(\vec{Q}) e^{i\vec{Q}\cdot\vec{r_n}} \sum_m f_m^*(\vec{Q}) e^{-i\vec{Q}\cdot\vec{r_m}} = \sum_{n,m} f_n(\vec{Q}) f_m^*(\vec{Q}) e^{i\vec{Q}\cdot(\vec{r_n}-\vec{r_m})}$$

$$= N\langle f(\vec{Q})^2\rangle + \sum_{n,m\neq n} f_m(\vec{Q}) f_n^*(\vec{Q}) e^{i\vec{Q}\cdot(\vec{r_n}-\vec{r_m})} = N\langle f(\vec{Q})^2\rangle + I_d(\vec{Q})$$

Pair distribution function

By treating powder diffraction patterns using total scattering methods it is possible to study disorder in crystalline materials as well as nanocrystalline materials

The theoretical approach is identical to that for short range order and SAXS, starting with the total scattered intensity from a multi-atomic system

$$I(\vec{Q}) = \sum_n f_n(\vec{Q}) e^{i\vec{Q}\cdot\vec{r_n}} \sum_m f_m^*(\vec{Q}) e^{-i\vec{Q}\cdot\vec{r_m}} = \sum_{n,m} f_n(\vec{Q}) f_m^*(\vec{Q}) e^{i\vec{Q}\cdot(\vec{r_n}-\vec{r_m})}$$
$$= N\langle f(\vec{Q})^2\rangle + \sum_{n,m\neq n} f_m(\vec{Q}) f_n^*(\vec{Q}) e^{i\vec{Q}\cdot(\vec{r_n}-\vec{r_m})} = N\langle f(\vec{Q})^2\rangle + I_d(\vec{Q})$$

where the first term is simply the self-scattering from all the atoms in the sample and we define the discrete scattering intensity, $I_d(\vec{Q})$, as:

Pair distribution function

By treating powder diffraction patterns using total scattering methods it is possible to study disorder in crystalline materials as well as nanocrystalline materials

The theoretical approach is identical to that for short range order and SAXS, starting with the total scattered intensity from a multi-atomic system

$$I(\vec{Q}) = \sum_n f_n(\vec{Q}) e^{i\vec{Q}\cdot\vec{r_n}} \sum_m f_m^*(\vec{Q}) e^{-i\vec{Q}\cdot\vec{r_m}} = \sum_{n,m} f_n(\vec{Q}) f_m^*(\vec{Q}) e^{i\vec{Q}\cdot(\vec{r_n}-\vec{r_m})}$$
$$= N\langle f(\vec{Q})^2\rangle + \sum_{n,m\neq n} f_m(\vec{Q}) f_n^*(\vec{Q}) e^{i\vec{Q}\cdot(\vec{r_n}-\vec{r_m})} = N\langle f(\vec{Q})^2\rangle + I_d(\vec{Q})$$

where the first term is simply the self-scattering from all the atoms in the sample and we define the discrete scattering intensity, $I_d(\vec{Q})$, as:

$$I_d(\vec{Q}) = I_c(\vec{Q}) - N\langle f(\vec{Q})^2\rangle = \sum_{n,m\neq n} f_m(\vec{Q}) f_n^*(\vec{Q}) e^{i\vec{Q}\cdot(\vec{r_n}-\vec{r_m})}$$

Scattering factor

The total scattering structure function, $S(\vec{Q})$ is given in terms of the discrete scattering intensity

Scattering factor

The total scattering structure function, $S(\vec{Q})$ is given in terms of the discrete scattering intensity

$$S(\vec{Q}) - 1 = \frac{I_d(\vec{Q})}{N\langle f \rangle^2}$$

Scattering factor

The total scattering structure function, $S(\vec{Q})$ is given in terms of the discrete scattering intensity

$$S(\vec{Q}) - 1 = \frac{I_d(\vec{Q})}{N\langle f \rangle^2} = \frac{1}{N\langle f \rangle^2} \sum_{n,m \neq n} f_m(\vec{Q}) f_n^*(\vec{Q}) e^{i\vec{Q}\cdot(\vec{r_n} - \vec{r_m})}$$

where $\langle f \rangle$ is the sample averaged scattering power

Scattering factor

The total scattering structure function, $S(\vec{Q})$ is given in terms of the discrete scattering intensity

$$S(\vec{Q}) - 1 = \frac{I_d(\vec{Q})}{N\langle f \rangle^2} = \frac{1}{N\langle f \rangle^2} \sum_{n,m \neq n} f_m(\vec{Q}) f_n^*(\vec{Q}) e^{i\vec{Q}\cdot(\vec{r_n} - \vec{r_m})}$$

where $\langle f \rangle$ is the sample averaged scattering power

if $\vec{Q}$ is taken to be in the $\hat{z}$ direction and the sample is assumed to be isotropic, angular averaging gives

Scattering factor

The total scattering structure function, $S(\vec{Q})$ is given in terms of the discrete scattering intensity

$$S(\vec{Q}) - 1 = \frac{I_d(\vec{Q})}{N\langle f \rangle^2} = \frac{1}{N\langle f \rangle^2} \sum_{n,m \neq n} f_m(\vec{Q}) f_n^*(\vec{Q}) e^{i\vec{Q}\cdot(\vec{r_n} - \vec{r_m})}$$

where $\langle f \rangle$ is the sample averaged scattering power

if $\vec{Q}$ is taken to be in the $\hat{z}$ direction and the sample is assumed to be isotropic, angular averaging gives

$$S(Q) - 1 = \frac{1}{N\langle f \rangle^2} \sum_{n,m \neq n} f_m(Q) f_n^*(Q) \frac{\sin Q r_{mn}}{Q r_{mn}}$$

Scattering factor

The total scattering structure function, $S(\vec{Q})$ is given in terms of the discrete scattering intensity

$$S(\vec{Q}) - 1 = \frac{I_d(\vec{Q})}{N\langle f \rangle^2} = \frac{1}{N\langle f \rangle^2} \sum_{n,m \neq n} f_m(\vec{Q}) f_n^*(\vec{Q}) e^{i\vec{Q}\cdot(\vec{r_n} - \vec{r_m})}$$

where $\langle f \rangle$ is the sample averaged scattering power

if $\vec{Q}$ is taken to be in the $\hat{z}$ direction and the sample is assumed to be isotropic, angular averaging gives

$$S(Q) - 1 = \frac{1}{N\langle f \rangle^2} \sum_{n,m \neq n} f_m(Q) f_n^*(Q) \frac{\sin Q r_{mn}}{Q r_{mn}}$$

and the reduced total scattering structure function, $F(Q)$ is

Scattering factor

The total scattering structure function, $S(\vec{Q})$ is given in terms of the discrete scattering intensity

$$S(\vec{Q}) - 1 = \frac{I_d(\vec{Q})}{N\langle f \rangle^2} = \frac{1}{N\langle f \rangle^2} \sum_{n,m \neq n} f_m(\vec{Q}) f_n^*(\vec{Q}) e^{i\vec{Q}\cdot(\vec{r_n} - \vec{r_m})}$$

where $\langle f \rangle$ is the sample averaged scattering power

if $\vec{Q}$ is taken to be in the $\hat{z}$ direction and the sample is assumed to be isotropic, angular averaging gives

$$S(Q) - 1 = \frac{1}{N\langle f \rangle^2} \sum_{n,m \neq n} f_m(Q) f_n^*(Q) \frac{\sin Q r_{mn}}{Q r_{mn}}$$

and the reduced total scattering structure function, $F(Q)$ is

$$F(Q) = Q[S(Q) - 1]$$

Scattering factor

The total scattering structure function, $S(\vec{Q})$ is given in terms of the discrete scattering intensity

$$S(\vec{Q}) - 1 = \frac{I_d(\vec{Q})}{N\langle f \rangle^2} = \frac{1}{N\langle f \rangle^2} \sum_{n,m \neq n} f_m(\vec{Q}) f_n^*(\vec{Q}) e^{i\vec{Q}\cdot(\vec{r_n} - \vec{r_m})}$$

where $\langle f \rangle$ is the sample averaged scattering power

if $\vec{Q}$ is taken to be in the $\hat{z}$ direction and the sample is assumed to be isotropic, angular averaging gives

$$S(Q) - 1 = \frac{1}{N\langle f \rangle^2} \sum_{n,m \neq n} f_m(Q) f_n^*(Q) \frac{\sin Q r_{mn}}{Q r_{mn}}$$

and the reduced total scattering structure function, $F(Q)$ is

$$F(Q) = Q[S(Q) - 1] = \frac{1}{N\langle f \rangle^2} \sum_{n,m \neq n} f_m(Q) f_n^*(Q) \frac{\sin Q r_{mn}}{r_{mn}}$$

PDF modeling

$$F(Q) = Q[S(Q) - 1] = \frac{1}{N\langle f \rangle^2} \sum_{n,m \neq n} f_m(Q) f_n^*(Q) \frac{\sin Q r_{mn}}{r_{mn}}$$

PDF modeling

$$F(Q) = Q[S(Q) - 1] = \frac{1}{N\langle f \rangle^2} \sum_{n,m \neq n} f_m(Q) f_n^*(Q) \frac{\sin Q r_{mn}}{r_{mn}}$$

The experimental pair distribution function, $G(r)$ is computed by taking the sine-Fourier transform

PDF modeling

$$F(Q) = Q[S(Q) - 1] = \frac{1}{N\langle f \rangle^2} \sum_{n,m \neq n} f_m(Q) f_n^*(Q) \frac{\sin Q r_{mn}}{r_{mn}}$$

The experimental pair distribution function, $G(r)$ is computed by taking the sine-Fourier transform

$$G(r) = \frac{2}{\pi} \int_{Q_{min}}^{Q_{max}} F(Q) \sin Qr \, dQ$$

PDF modeling

$$F(Q) = Q[S(Q) - 1] = \frac{1}{N\langle f \rangle^2} \sum_{n,m \neq n} f_m(Q) f_n^*(Q) \frac{\sin Q r_{mn}}{r_{mn}}$$

The experimental pair distribution function, $G(r)$ is computed by taking the sine-Fourier transform

$$G(r) = \frac{2}{\pi} \int_{Q_{min}}^{Q_{max}} F(Q) \sin Qr \, dQ$$

but $G(r)$ can be calculated from a known structural model

PDF modeling

$$F(Q) = Q[S(Q) - 1] = \frac{1}{N\langle f \rangle^2} \sum_{n,m \neq n} f_m(Q) f_n^*(Q) \frac{\sin Q r_{mn}}{r_{mn}}$$

The experimental pair distribution function, $G(r)$ is computed by taking the sine-Fourier transform

$$G(r) = \frac{2}{\pi} \int_{Q_{min}}^{Q_{max}} F(Q) \sin Qr \, dQ$$

but $G(r)$ can be calculated from a known structural model

$$G(r) = 4\pi r[\rho(r) - \rho_0],$$

PDF modeling

$$F(Q) = Q[S(Q) - 1] = \frac{1}{N\langle f \rangle^2} \sum_{n,m \neq n} f_m(Q) f_n^*(Q) \frac{\sin Q r_{mn}}{r_{mn}}$$

The experimental pair distribution function, $G(r)$ is computed by taking the sine-Fourier transform

$$G(r) = \frac{2}{\pi} \int_{Q_{min}}^{Q_{max}} F(Q) \sin Qr \, dQ$$

but $G(r)$ can be calculated from a known structural model

$$G(r) = 4\pi r[\rho(r) - \rho_0], \qquad \rho(r) = \frac{1}{4\pi r^2 N\langle f \rangle^2} \sum_{n,m \neq n} Z_m Z_n \delta(r - r_{mn})$$

PDF modeling

$$F(Q) = Q[S(Q) - 1] = \frac{1}{N\langle f \rangle^2} \sum_{n,m \neq n} f_m(Q) f_n^*(Q) \frac{\sin Q r_{mn}}{r_{mn}}$$

The experimental pair distribution function, $G(r)$ is computed by taking the sine-Fourier transform

$$G(r) = \frac{2}{\pi} \int_{Q_{min}}^{Q_{max}} F(Q) \sin Qr \, dQ$$

but $G(r)$ can be calculated from a known structural model

$$G(r) = 4\pi r[\rho(r) - \rho_0], \qquad \rho(r) = \frac{1}{4\pi r^2 N\langle f \rangle^2} \sum_{n,m \neq n} Z_m Z_n \delta(r - r_{mn})$$

where ρ_0 is the atomic number density, $\rho(r)$ is the atomic pair density, and r_{mn} is the distance between atoms m and n

PDF modeling

$$F(Q) = Q[S(Q) - 1] = \frac{1}{N\langle f \rangle^2} \sum_{n,m \neq n} f_m(Q) f_n^*(Q) \frac{\sin Q r_{mn}}{r_{mn}}$$

The experimental pair distribution function, $G(r)$ is computed by taking the sine-Fourier transform

$$G(r) = \frac{2}{\pi} \int_{Q_{min}}^{Q_{max}} F(Q) \sin Qr \, dQ$$

but $G(r)$ can be calculated from a known structural model

$$G(r) = 4\pi r[\rho(r) - \rho_0], \qquad \rho(r) = \frac{1}{4\pi r^2 N\langle f \rangle^2} \sum_{n,m \neq n} Z_m Z_n \delta(r - r_{mn})$$

where ρ_0 is the atomic number density, $\rho(r)$ is the atomic pair density, and r_{mn} is the distance between atoms m and n

So what does the pair distribution function look like in practice?

PDF processing: $F(Q)$ and $G(r)$

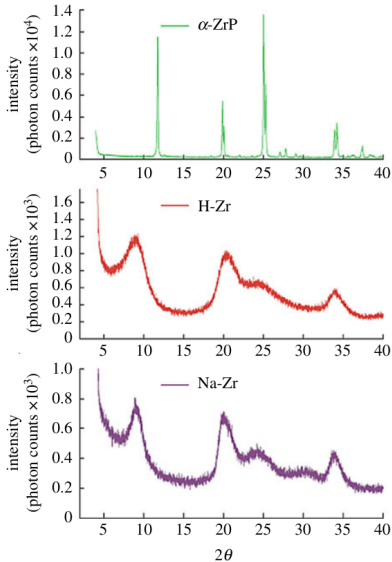

"Local environment of terbium(III) ions in layered nanocrystalline zirconium(IV) phosphate – phosphate ion exchange materials," M.W. Terban, et al. *Inorg. Chem.* **56**, 8837-8846 (2017).

PDF processing: $F(Q)$ and $G(r)$

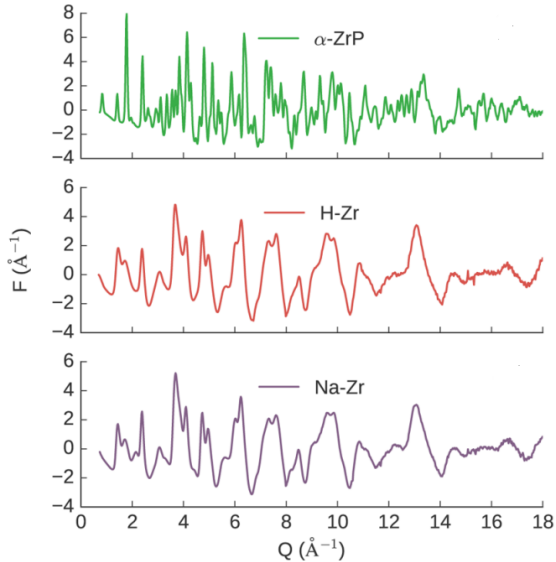

The broad peaks of nanoparticle systems still contains information once processed into the reduced total scattering function

"Local environment of terbium(III) ions in layered nanocrystalline zirconium(IV) phosphate – phosphate ion exchange materials," M.W. Terban, et al. *Inorg. Chem.* **56**, 8837-8846 (2017).

PDF processing: $F(Q)$ and $G(r)$

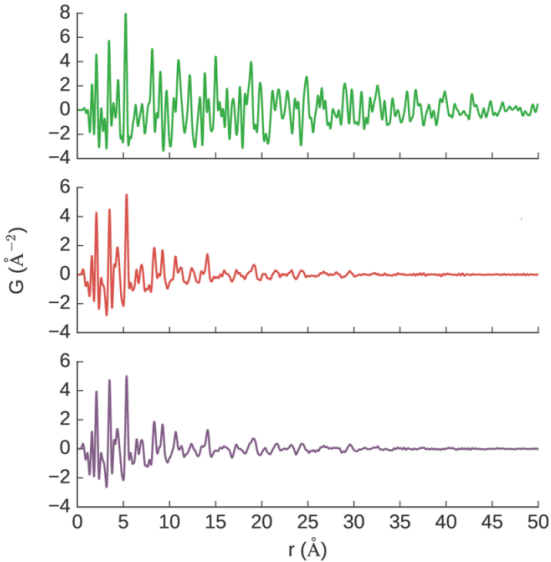

The broad peaks of nanoparticle systems still contains information once processed into the reduced total scattering function

When Fourier transformed, the significant differences in crystalline and nanoparticulate samples are obvious

"Local environment of terbium(III) ions in layered nanocrystalline zirconium(IV) phosphate – phosphate ion exchange materials," M.W. Terban, et al. *Inorg. Chem.* **56**, 8837-8846 (2017).

PDF structure of CdSe nanoparticles

The goal of this study was to compare the PDF structures of CdSe nanoparticles of various sizes with the results obtained from traditional analysis of optical data and electron microscopy

"Quantitative size-dependent structure and strain determination of CdSe nanoparticles using atomic pair distribution function analysis," A.S. Masadeh, et al. *Phys. Rev. B* **76**, 115413 (2007).

PDF structure of CdSe nanoparticles

The goal of this study was to compare the PDF structures of CdSe nanoparticles of various sizes with the results obtained from traditional analysis of optical data and electron microscopy

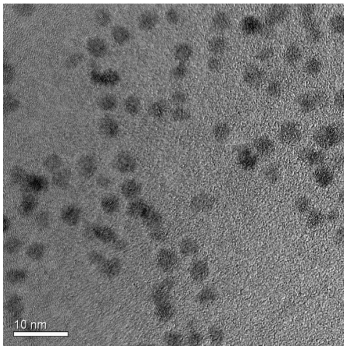

Nanoparticles of of three different sizes were obtained by changing the nucleation time from 1200 s (left)

"Quantitative size-dependent structure and strain determination of CdSe nanoparticles using atomic pair distribution function analysis," A.S. Masadeh, et al. *Phys. Rev. B* **76**, 115413 (2007).

PDF structure of CdSe nanoparticles

The goal of this study was to compare the PDF structures of CdSe nanoparticles of various sizes with the results obtained from traditional analysis of optical data and electron microscopy

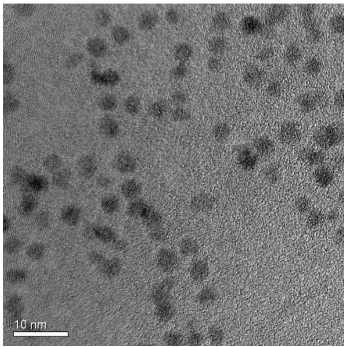

Nanoparticles of of three different sizes were obtained by changing the nucleation time from 1200 s (left) to 15 s (right) during synthesis

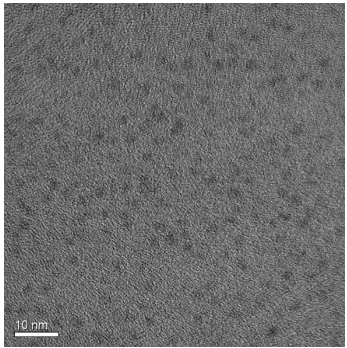

"Quantitative size-dependent structure and strain determination of CdSe nanoparticles using atomic pair distribution function analysis," A.S. Masadeh, et al. *Phys. Rev. B* **76**, 115413 (2007).

PDF structure of CdSe nanoparticles

The goal of this study was to compare the PDF structures of CdSe nanoparticles of various sizes with the results obtained from traditional analysis of optical data and electron microscopy

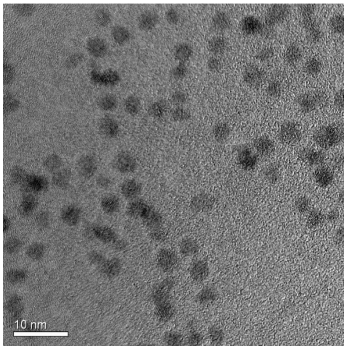

Nanoparticles of of three different sizes were obtained by changing the nucleation time from 1200 s (left) to 15 s (right) during synthesis

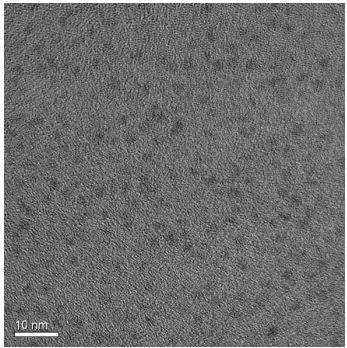

Optical absorbance and fluorescence indicates particle sizes ranging from 3.5 nm to 2.0 nm

"Quantitative size-dependent structure and strain determination of CdSe nanoparticles using atomic pair distribution function analysis," A.S. Masadeh, et al. *Phys. Rev. B* **76**, 115413 (2007).

PDF data collection

Diffraction data were collected at APS beamline 6-IDD with incident 87 keV x-rays on a 2D image plate detector

"Quantitative size-dependent structure and strain determination of CdSe nanoparticles using atomic pair distribution function analysis," A.S. Masadeh, et al. *Phys. Rev. B* **76**, 115413 (2007).

PDF data collection

Diffraction data were collected at APS beamline 6-IDD with incident 87 keV x-rays on a 2D image plate detector

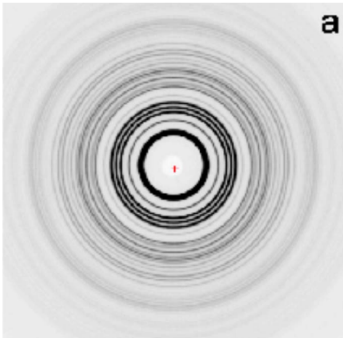

Data were collected on bulk CdSe (left)

"Quantitative size-dependent structure and strain determination of CdSe nanoparticles using atomic pair distribution function analysis," A.S. Masadeh, et al. *Phys. Rev. B* **76**, 115413 (2007).

PDF data collection

Diffraction data were collected at APS beamline 6-IDD with incident 87 keV x-rays on a 2D image plate detector

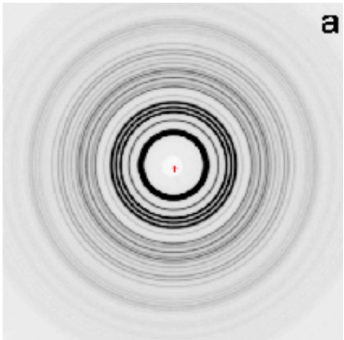

Data were collected on bulk CdSe (left) and the CdSe nanoparticles (right) then azimuthally integrated to get the powder pattern

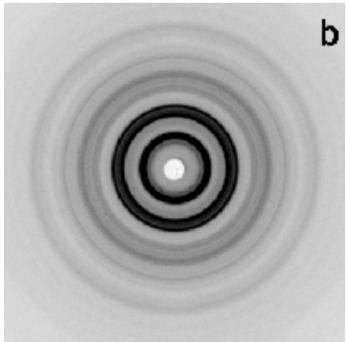

"Quantitative size-dependent structure and strain determination of CdSe nanoparticles using atomic pair distribution function analysis," A.S. Masadeh, et al. *Phys. Rev. B* **76**, 115413 (2007).

$F(Q)$ and $G(r)$

The data for bulk and nanoparticle samples was processed to obtain $F(Q)$ and $G(r)$ in preparation for structural modeling

"Quantitative size-dependent structure and strain determination of CdSe nanoparticles using atomic pair distribution function analysis," A.S. Masadeh, et al. *Phys. Rev. B* **76**, 115413 (2007).

$F(Q)$ and $G(r)$

The data for bulk and nanoparticle samples was processed to obtain $F(Q)$ and $G(r)$ in preparation for structural modeling

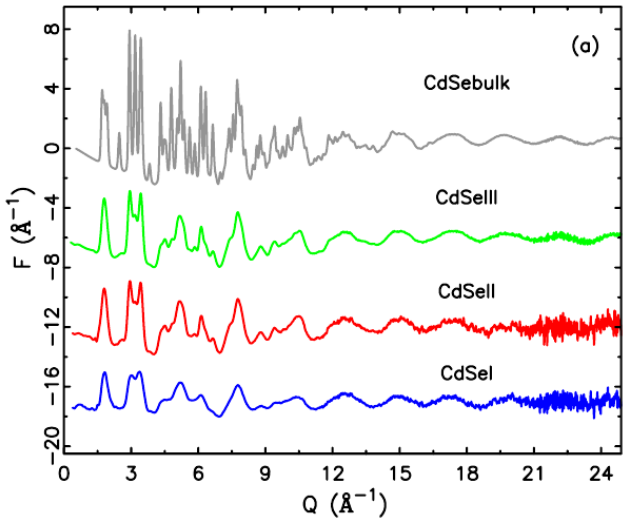

"Quantitative size-dependent structure and strain determination of CdSe nanoparticles using atomic pair distribution function analysis," A.S. Masadeh, et al. *Phys. Rev. B* **76**, 115413 (2007).

$F(Q)$ and $G(r)$

The data for bulk and nanoparticle samples was processed to obtain $F(Q)$ and $G(r)$ in preparation for structural modeling

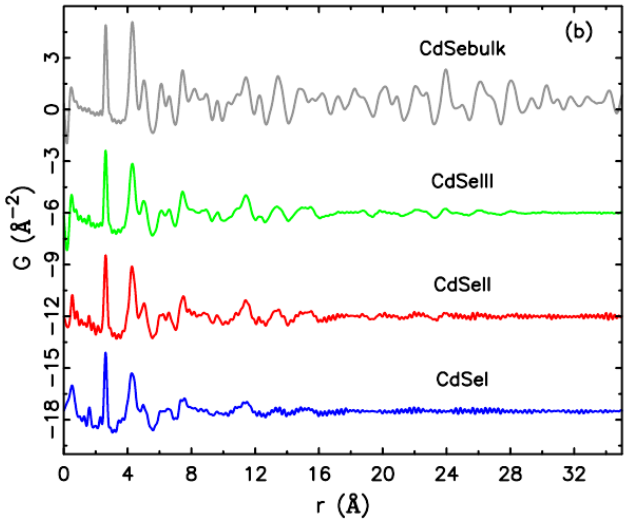

"Quantitative size-dependent structure and strain determination of CdSe nanoparticles using atomic pair distribution function analysis," A.S. Masadeh, et al. *Phys. Rev. B* **76**, 115413 (2007).

$F(Q)$ and $G(r)$

The data for bulk and nanoparticle samples was processed to obtain $F(Q)$ and $G(r)$ in preparation for structural modeling

The particle size progression shows in the range over which the $G(r)$ has distinct peak structure

"Quantitative size-dependent structure and strain determination of CdSe nanoparticles using atomic pair distribution function analysis," A.S. Masadeh, et al. *Phys. Rev. B* **76**, 115413 (2007).

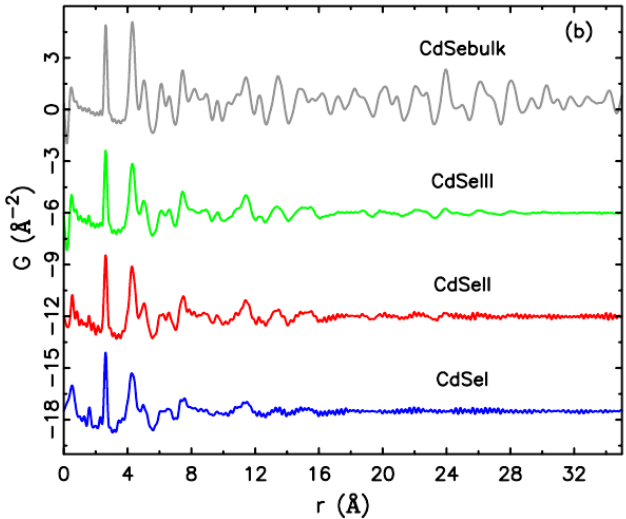

Initial modeling

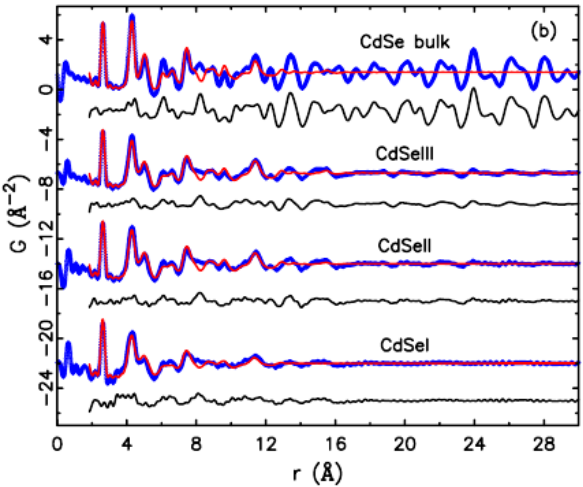

The first fit to the data uses the wurtzite structure which has ABAB stacking of hexagonal planes

"Quantitative size-dependent structure and strain determination of CdSe nanoparticles using atomic pair distribution function analysis," A.S. Masadeh, et al. *Phys. Rev. B* **76**, 115413 (2007).

Initial modeling

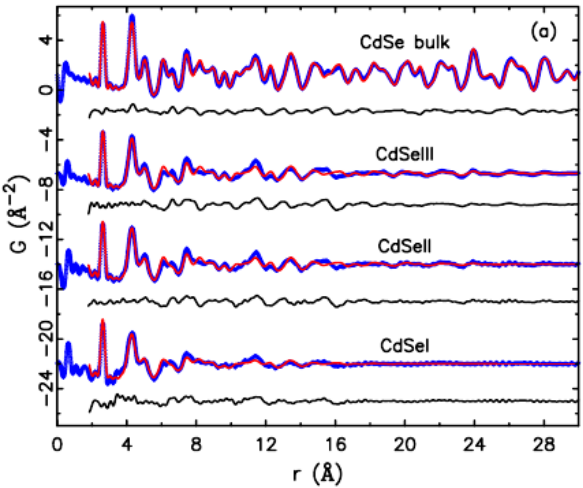

The first fit to the data uses the wurtzite structure which has ABAB stacking of hexagonal planes

The second uses the zinc blende structure with ABC stacking

"Quantitative size-dependent structure and strain determination of CdSe nanoparticles using atomic pair distribution function analysis," A.S. Masadeh, et al. *Phys. Rev. B* **76**, 115413 (2007).

Initial modeling

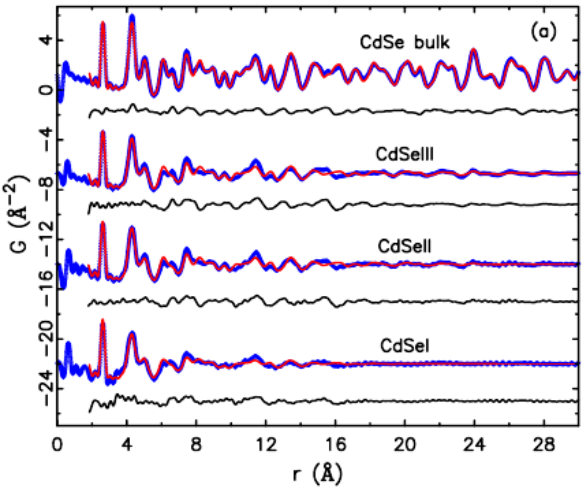

The first fit to the data uses the wurtzite structure which has ABAB stacking of hexagonal planes

The second uses the zinc blende structure with ABC stacking

While the zinc blende does slightly better at fitting the experimental data, it is clear that neither is perfect for the bulk or the nanoparticles

"Quantitative size-dependent structure and strain determination of CdSe nanoparticles using atomic pair distribution function analysis," A.S. Masadeh, et al. *Phys. Rev. B* **76**, 115413 (2007).

Initial modeling

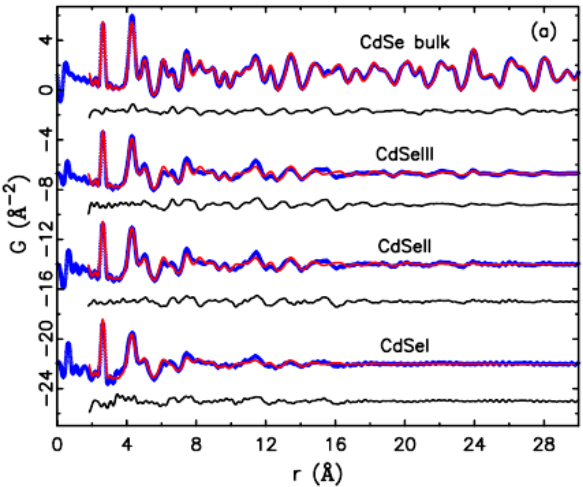

The first fit to the data uses the wurtzite structure which has ABAB stacking of hexagonal planes

The second uses the zinc blende structure with ABC stacking

While the zinc blende does slightly better at fitting the experimental data, it is clear that neither is perfect for the bulk or the nanoparticles

It is likely that a better fit can be obtained using a mixture of the two stacking arrangements

"Quantitative size-dependent structure and strain determination of CdSe nanoparticles using atomic pair distribution function analysis," A.S. Masadeh, et al. *Phys. Rev. B* **76**, 115413 (2007).

Final structural models

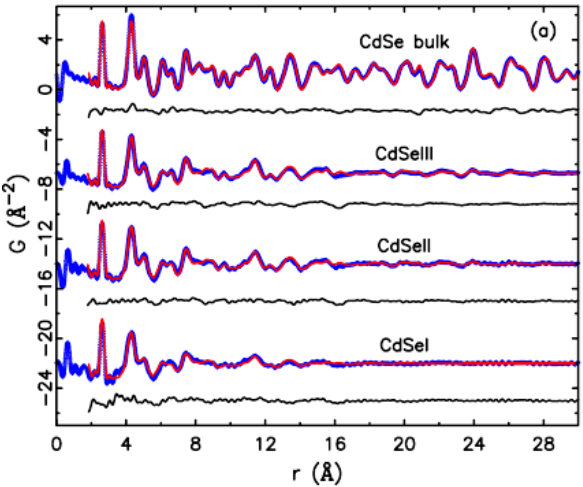

A fit using both wurtzite and zinc blende fits much better for all particles

"Quantitative size-dependent structure and strain determination of CdSe nanoparticles using atomic pair distribution function analysis," A.S. Masadeh, et al. *Phys. Rev. B* **76**, 115413 (2007).

Final structural models

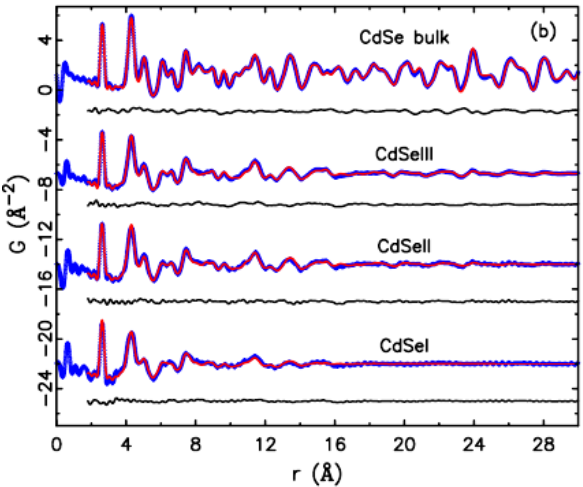

A fit using both wurtzite and zinc blende fits much better for all particles

An even better fit is obtained by including a variable number of stacking faults in the model (i.e. transitions between wurtzite and zinc blende structures)

"Quantitative size-dependent structure and strain determination of CdSe nanoparticles using atomic pair distribution function analysis," A.S. Masadeh, et al. *Phys. Rev. B* **76**, 115413 (2007).

Final structural models

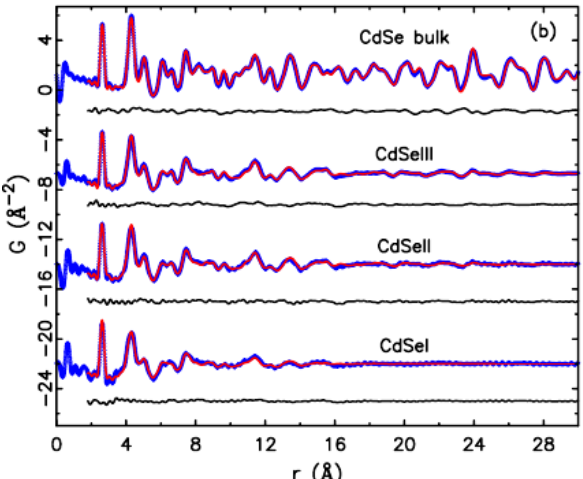

A fit using both wurtzite and zinc blende fits much better for all particles

An even better fit is obtained by including a variable number of stacking faults in the model (i.e. transitions between wurtzite and zinc blende structures)

The final values obtained in the fitting give particle sizes consistent with TEM and optical measurements. The fits also show that the bulk sample has only about 33% stacking faults while the nanoparticles have 50%

"Quantitative size-dependent structure and strain determination of CdSe nanoparticles using atomic pair distribution function analysis," A.S. Masadeh, et al. *Phys. Rev. B* **76**, 115413 (2007).

Scattering intensity from a crystallite

A small crystal fully illuminated by a monochromatic x-ray beam has differential scattering cross-section

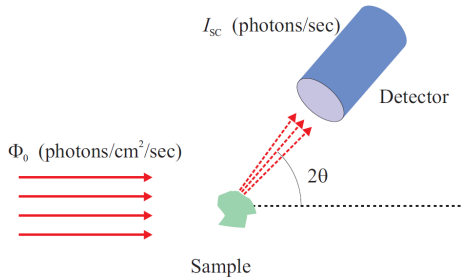

Scattering intensity from a crystallite

A small crystal fully illuminated by a monochromatic x-ray beam has differential scattering cross-section

$$\left(\frac{d\sigma}{d\Omega}\right) = r_0^2 P |F(\vec{Q})|^2 N v_c^* \delta(\vec{Q} - \vec{G})$$

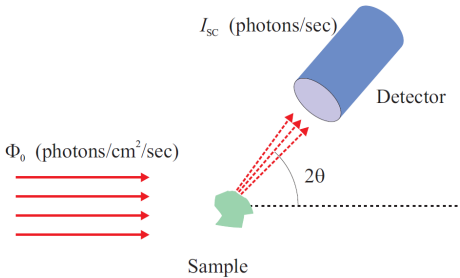

Scattering intensity from a crystallite

A small crystal fully illuminated by a monochromatic x-ray beam has differential scattering cross-section

$$\left(\frac{d\sigma}{d\Omega}\right) = r_0^2 P |F(\vec{Q})|^2 N v_c^* \delta(\vec{Q} - \vec{G})$$

the Bragg peak is not infinitely narrow ($\propto 1/N$) so the scattered wavevector ($\vec{k}'$) can be slightly divergent and the crystal must be rotated to collect the integrated intensity of the reflection

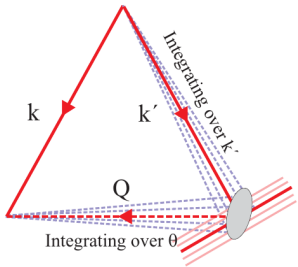

Scattering intensity from a crystallite

A small crystal fully illuminated by a monochromatic x-ray beam has differential scattering cross-section

$$\left(\frac{d\sigma}{d\Omega}\right) = r_0^2 P |F(\vec{Q})|^2 N v_c^* \delta(\vec{Q} - \vec{G})$$

the Bragg peak is not infinitely narrow ($\propto 1/N$) so the scattered wavevector ($\vec{k}'$) can be slightly divergent and the crystal must be rotated to collect the integrated intensity of the reflection

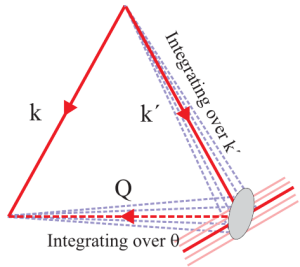

The intensity expression must be integrated over both $\vec{k}'$ and θ to compute what the detector measures

Scattering intensity from a crystallite

A small crystal fully illuminated by a monochromatic x-ray beam has differential scattering cross-section

$$\left(\frac{d\sigma}{d\Omega}\right) = r_0^2 P |F(\vec{Q})|^2 N v_c^* \delta(\vec{Q} - \vec{G})$$

the Bragg peak is not infinitely narrow ($\propto 1/N$) so the scattered wavevector ($\vec{k}'$) can be slightly divergent and the crystal must be rotated to collect the integrated intensity of the reflection

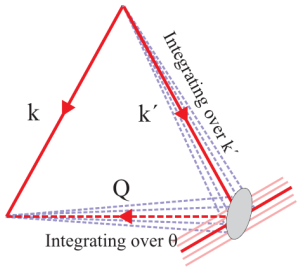

The intensity expression must be integrated over both $\vec{k}'$ and θ to compute what the detector measures

$$\int \delta(\vec{Q} - \vec{G}) d\vec{k}' = \int \delta(\vec{k} - \vec{k}' - \vec{G}) d\vec{k}'$$

Scattering intensity from a crystallite

A small crystal fully illuminated by a monochromatic x-ray beam has differential scattering cross-section

$$\left(\frac{d\sigma}{d\Omega}\right) = r_0^2 P |F(\vec{Q})|^2 N v_c^* \delta(\vec{Q} - \vec{G})$$

the Bragg peak is not infinitely narrow ($\propto 1/N$) so the scattered wavevector ($\vec{k}'$) can be slightly divergent and the crystal must be rotated to collect the integrated intensity of the reflection

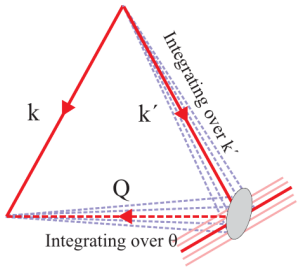

The intensity expression must be integrated over both $\vec{k}'$ and θ to compute what the detector measures

$$\int \delta(\vec{Q} - \vec{G}) d\vec{k}' = \int \delta(\vec{k} - \vec{k}' - \vec{G}) d\vec{k}' = \cdots$$

Scattering intensity from a crystallite

A small crystal fully illuminated by a monochromatic x-ray beam has differential scattering cross-section

$$\left(\frac{d\sigma}{d\Omega}\right) = r_0^2 P |F(\vec{Q})|^2 N v_c^* \delta(\vec{Q} - \vec{G})$$

the Bragg peak is not infinitely narrow ($\propto 1/N$) so the scattered wavevector ($\vec{k}'$) can be slightly divergent and the crystal must be rotated to collect the integrated intensity of the reflection

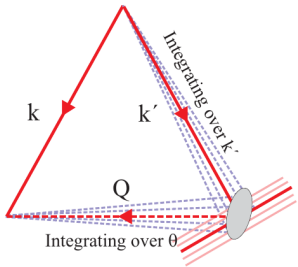

The intensity expression must be integrated over both $\vec{k}'$ and θ to compute what the detector measures

$$\int \delta(\vec{Q} - \vec{G}) d\vec{k}' = \int \delta(\vec{k} - \vec{k}' - \vec{G}) d\vec{k}' = \cdots = \frac{2}{k} \delta(G^2 - 2kG \sin\theta)$$

Lorentz factor

After the integration over $\vec{k}'$, the differential scattering cross section must still be integrated over θ

$$\left(\frac{d\sigma}{d\Omega}\right) = r_0^2 P |F(\vec{Q})|^2 N v_c^* \frac{2}{k} \delta(G^2 - 2kG\sin\theta)$$

Lorentz factor

After the integration over $\vec{k}'$, the differential scattering cross section must still be integrated over θ

$$\left(\frac{d\sigma}{d\Omega}\right) = r_0^2 P |F(\vec{Q})|^2 N v_c^* \frac{2}{k} \delta(G^2 - 2kG\sin\theta)$$

$$\int \delta(G^2 - 2kG\sin\theta) d\theta = \cdots$$

Lorentz factor

After the integration over $\vec{k}'$, the differential scattering cross section must still be integrated over θ

$$\left(\frac{d\sigma}{d\Omega}\right) = r_0^2 P |F(\vec{Q})|^2 N v_c^* \frac{2}{k} \delta(G^2 - 2kG\sin\theta)$$

$$\int \delta(G^2 - 2kG\sin\theta) d\theta = \cdots = \frac{-1}{2k^2 \sin 2\theta}$$

Lorentz factor

After the integration over $\vec{k}'$, the differential scattering cross section must still be integrated over θ

$$\left(\frac{d\sigma}{d\Omega}\right) = r_0^2 P |F(\vec{Q})|^2 N v_c^* \frac{2}{k} \delta(G^2 - 2kG\sin\theta)$$

$$\int \delta(G^2 - 2kG\sin\theta) d\theta = \cdots = \frac{-1}{2k^2 \sin 2\theta}$$

$$\left(\frac{d\sigma}{d\Omega}\right) = r_0^2 P |F(\vec{Q})|^2 N v_c^* \frac{2}{k} \left|\frac{-1}{2k^2 \sin 2\theta}\right|$$

Lorentz factor

After the integration over $\vec{k}'$, the differential scattering cross section must still be integrated over θ

$$\left(\frac{d\sigma}{d\Omega}\right) = r_0^2 P |F(\vec{Q})|^2 N v_c^* \frac{2}{k} \delta(G^2 - 2kG\sin\theta)$$

$$\int \delta(G^2 - 2kG\sin\theta) d\theta = \cdots = \frac{-1}{2k^2 \sin 2\theta}$$

$$\left(\frac{d\sigma}{d\Omega}\right) = r_0^2 P |F(\vec{Q})|^2 N v_c^* \frac{2}{k} \left|\frac{-1}{2k^2 \sin 2\theta}\right| = r_0^2 P |F(\vec{Q})|^2 N \frac{\lambda^3}{v_c \sin 2\theta}$$

$$I_{SC} = \Phi_0 r_0^2 P |F(\vec{Q})|^2 N \frac{\lambda^3}{v_c \sin 2\theta}$$

Lorentz factor

After the integration over $\vec{k}'$, the differential scattering cross section must still be integrated over θ

$$\left(\frac{d\sigma}{d\Omega}\right) = r_0^2 P |F(\vec{Q})|^2 N v_c^* \frac{2}{k} \delta(G^2 - 2kG\sin\theta)$$

$$\int \delta(G^2 - 2kG\sin\theta) d\theta = \cdots = \frac{-1}{2k^2 \sin 2\theta}$$

$$\left(\frac{d\sigma}{d\Omega}\right) = r_0^2 P |F(\vec{Q})|^2 N v_c^* \frac{2}{k} \left|\frac{-1}{2k^2 \sin 2\theta}\right| = r_0^2 P |F(\vec{Q})|^2 N \frac{\lambda^3}{v_c \sin 2\theta}$$

$$I_{SC} = \Phi_0 r_0^2 P |F(\vec{Q})|^2 N \frac{\lambda^3}{v_c \sin 2\theta}$$

scattering by each electron is given by $r_0^2 P$ while The scattering from each of N unit cells is $|F(\vec{Q})|^2$ and the last term is the Lorentz factor

Extinction

Most small crystals are not "perfect" but can be seen as composed of small blocks with misalignments of the order of $\leq 0.1^{\circ}$

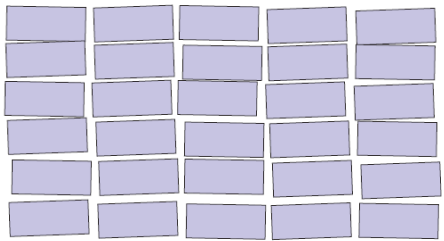

Extinction

Most small crystals are not "perfect" but can be seen as composed of small blocks with misalignments of the order of $\leq 0.1^\circ$

if some of these perfect blocks are shadowed by other blocks which intercept and scatter the x-rays, then *secondary extinction* effects must be considered

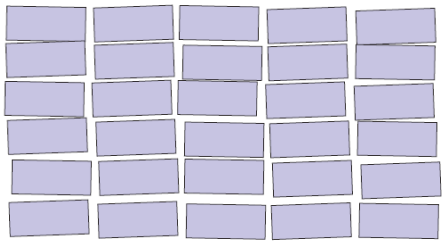

Extinction

Most small crystals are not "perfect" but can be seen as composed of small blocks with misalignments of the order of $\leq 0.1^\circ$

if some of these perfect blocks are shadowed by other blocks which intercept and scatter the x-rays, then *secondary extinction* effects must be considered

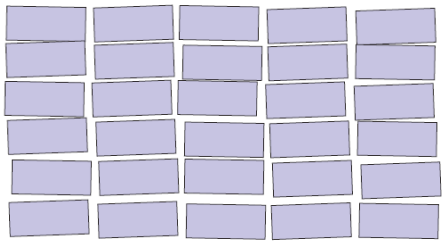

Primary extinction effects arise when there is a large perfect crystal as will be seen later on

Absorption

Absorption effects have been ignored so far but can have a significant effect

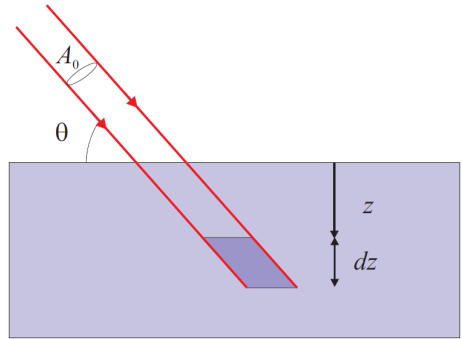

Absorption

Absorption effects have been ignored so far but can have a significant effect

consider a mosaic crystal with $N = N' \times N_{mb}$ mosaic blocks

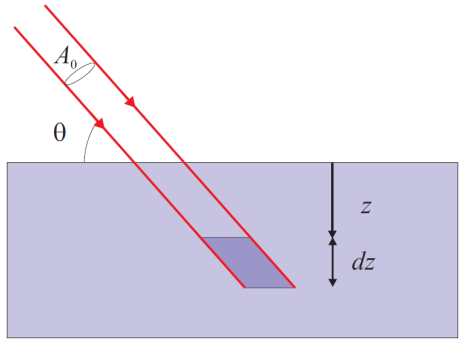

Absorption

Absorption effects have been ignored so far but can have a significant effect

consider a mosaic crystal with $N = N' \times N_{mb}$ mosaic blocks

the number of mosaic blocks illuminated by a beam of cross sectional area A_0 is

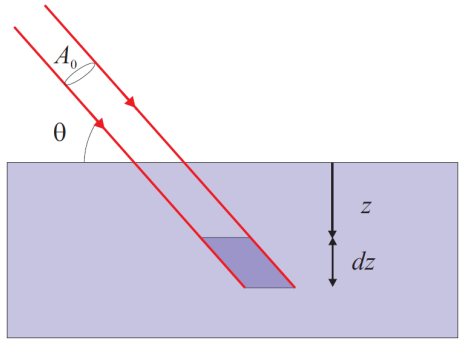

Absorption

Absorption effects have been ignored so far but can have a significant effect

consider a mosaic crystal with $N = N' \times N_{mb}$ mosaic blocks

the number of mosaic blocks illuminated by a beam of cross sectional area A_0 is

$$N_{mb} = \frac{A_0 dz}{\sin\theta} \times \frac{1}{V'}$$

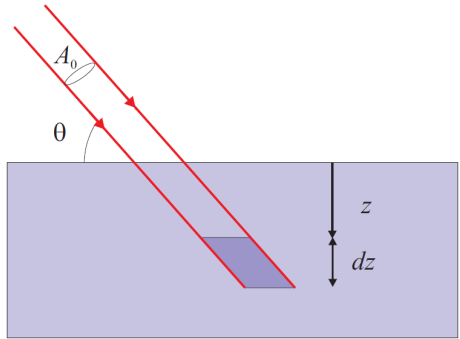

Absorption

Absorption effects have been ignored so far but can have a significant effect

consider a mosaic crystal with $N = N' \times N_{mb}$ mosaic blocks

the number of mosaic blocks illuminated by a beam of cross sectional area A_0 is

$$N_{mb} = \frac{A_0 dz}{\sin\theta} \times \frac{1}{V'}$$

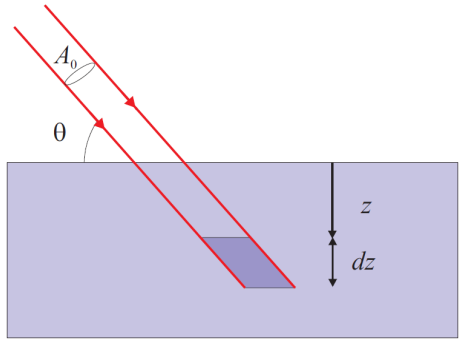

at a depth z, absorption reduces the beam intensity by a factor $e^{-2\mu z/\sin\theta}$ and the integrated intensity becomes

Absorption

Absorption effects have been ignored so far but can have a significant effect

consider a mosaic crystal with $N = N' \times N_{mb}$ mosaic blocks

the number of mosaic blocks illuminated by a beam of cross sectional area A_0 is

$$N_{mb} = \frac{A_0 dz}{\sin\theta} \times \frac{1}{V'}$$

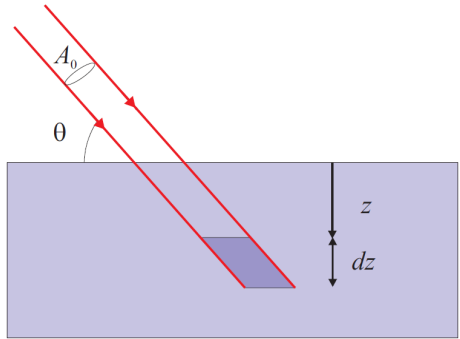

at a depth z, absorption reduces the beam intensity by a factor $e^{-2\mu z/\sin\theta}$ and the integrated intensity becomes

$$I_{SC} = \frac{\Phi_0 r_0^2 P |F(\vec{Q})|^2 \lambda^3}{v_c \sin 2\theta} N' \int_0^\infty e^{-2\mu z/\sin\theta} \frac{A_0 dz}{V' \sin\theta}$$

Absorption

Absorption effects have been ignored so far but can have a significant effect

consider a mosaic crystal with $N = N' \times N_{mb}$ mosaic blocks

the number of mosaic blocks illuminated by a beam of cross sectional area A_0 is

$$N_{mb} = \frac{A_0 dz}{\sin\theta} \times \frac{1}{V'}$$

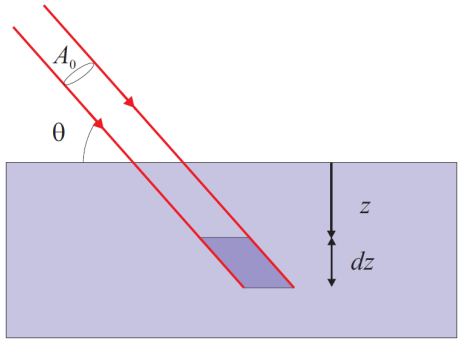

at a depth z, absorption reduces the beam intensity by a factor $e^{-2\mu z/\sin\theta}$ and the integrated intensity becomes

$$I_{SC} = \frac{\Phi_0 r_0^2 P |F(\vec{Q})|^2 \lambda^3}{v_c \sin 2\theta} N' \int_0^\infty e^{-2\mu z/\sin\theta} \frac{A_0 dz}{V' \sin\theta} = \cdots$$

Absorption

Absorption effects have been ignored so far but can have a significant effect

consider a mosaic crystal with $N = N' \times N_{mb}$ mosaic blocks

the number of mosaic blocks illuminated by a beam of cross sectional area A_0 is

$$N_{mb} = \frac{A_0 dz}{\sin\theta} \times \frac{1}{V'}$$

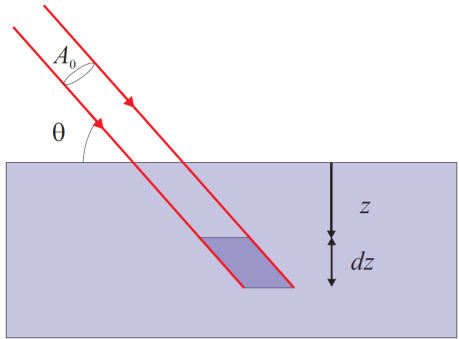

at a depth z, absorption reduces the beam intensity by a factor $e^{-2\mu z/\sin\theta}$ and the integrated intensity becomes

$$I_{SC} = \frac{\Phi_0 r_0^2 P |F(\vec{Q})|^2 \lambda^3}{v_c \sin 2\theta} N' \int_0^\infty e^{-2\mu z/\sin\theta} \frac{A_0 dz}{V' \sin\theta} = \cdots = \frac{1}{2\mu} \cdot \frac{\Phi_0 r_0^2 P |F(\vec{Q})|^2 \lambda^3}{v_c \sin 2\theta}$$

Kinematical vs. dynamical diffraction

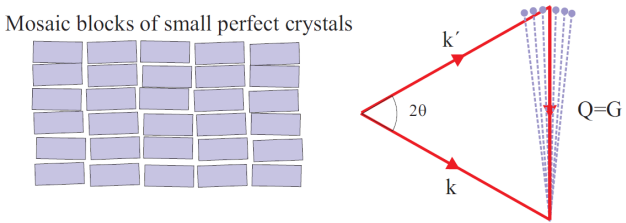

The kinematical approximation we have discussed so far applies to mosaic crystals. The size of the crystal is small enough that the wave field of the x-rays does not vary appreciably over the crystal.

Kinematical vs. dynamical diffraction

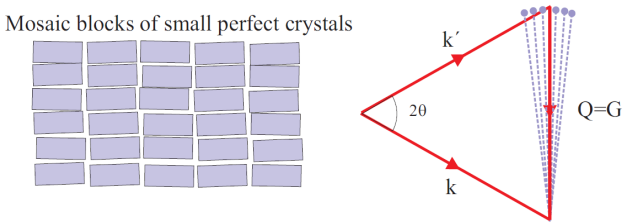

The kinematical approximation we have discussed so far applies to mosaic crystals. The size of the crystal is small enough that the wave field of the x-rays does not vary appreciably over the crystal.

For a perfect crystal, such as those used in monochromators, things are very different and we have to treat them specially using dynamical diffraction theory.

Kinematical vs. dynamical diffraction

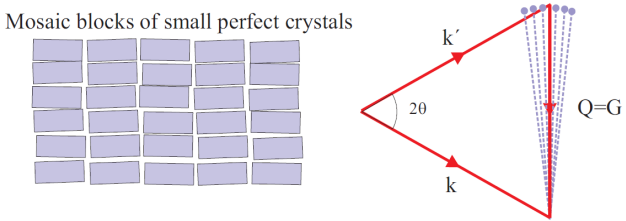

The kinematical approximation we have discussed so far applies to mosaic crystals. The size of the crystal is small enough that the wave field of the x-rays does not vary appreciably over the crystal.

For a perfect crystal, such as those used in monochromators, things are very different and we have to treat them specially using dynamical diffraction theory.

This theory takes into account multiple reflections, and attenuation of the x-ray beam as it propagates through the perfect crystal.

Bragg & Laue geometries

Bragg & Laue geometries

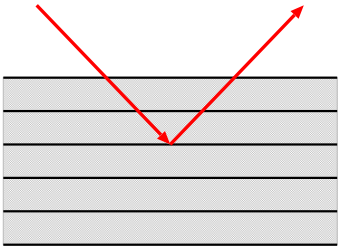

symmetric

⟵ Bragg

Bragg & Laue geometries

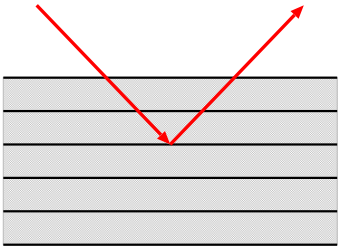

symmetric

⟵ Bragg

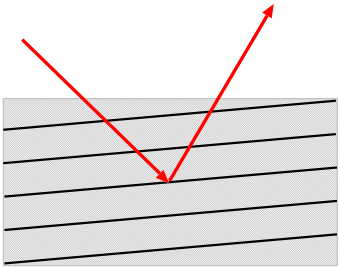

asymmetric

Bragg & Laue geometries

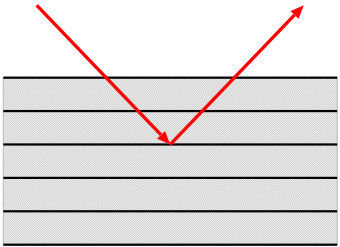

symmetric

⟵ Bragg

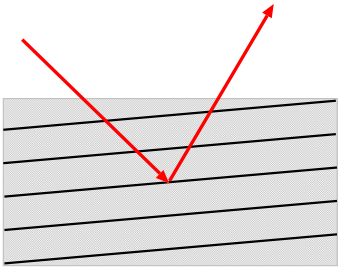

asymmetric

Bragg & Laue geometries

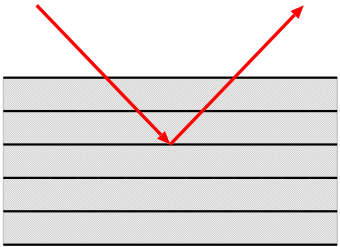

symmetric

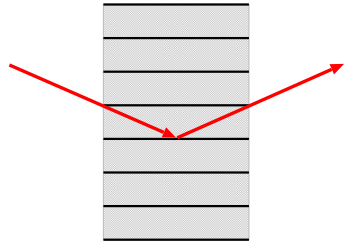

⟵ Bragg

Laue ⟶

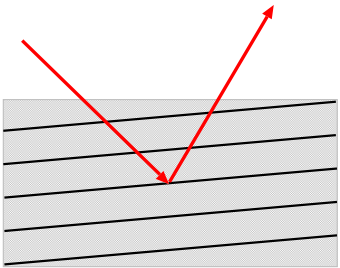

asymmetric

Bragg & Laue geometries

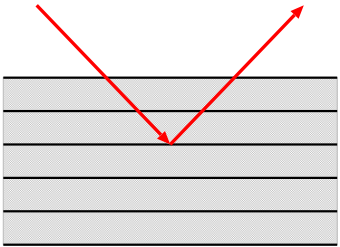

symmetric

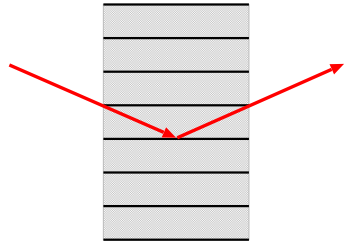

⟵ Bragg

Laue ⟶

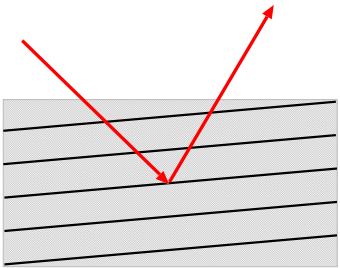

asymmetric

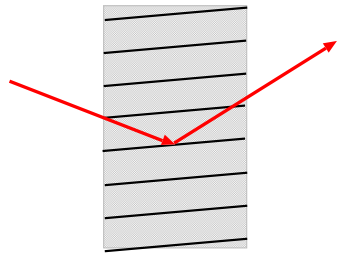

Scattering geometry

Consider symmetric Bragg geometry

Scattering geometry

Consider symmetric Bragg geometry

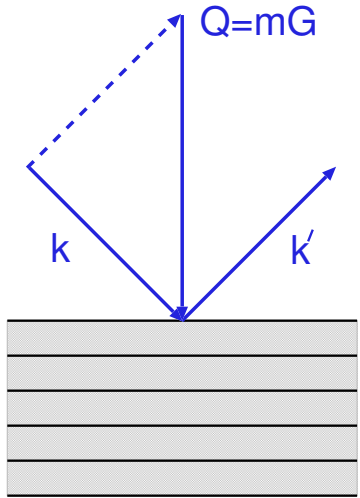

Scattering geometry

Consider symmetric Bragg geometry

We expect the crystal to diffract in an energy bandwidth defined by Δk

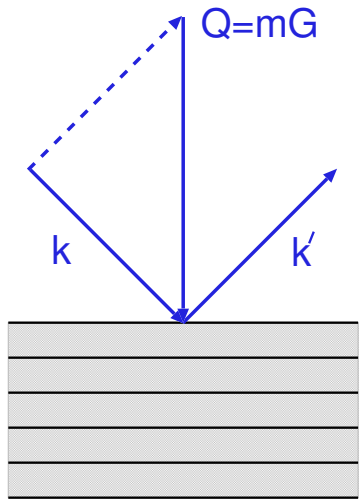

Scattering geometry

Consider symmetric Bragg geometry

We expect the crystal to diffract in an energy bandwidth defined by Δk

This defines a spread of scattering vectors such that

$$\zeta = \frac{\Delta Q}{Q} = \frac{\Delta k}{k}$$

called the relative energy or wavelength bandwidth

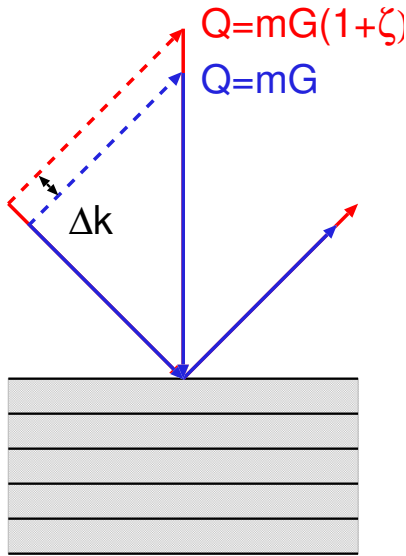

Darwin approach – single layer reflectivity

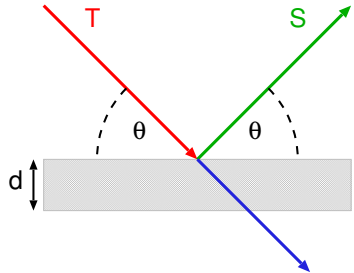

Darwin approach – single layer reflectivity

Consider a single thin slab with electron density ρ and thickness $d \ll \lambda$, the reflected and transmitted waves are functions of the incident wave

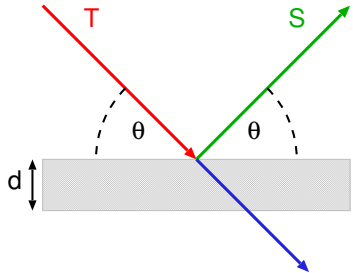

Darwin approach – single layer reflectivity

Consider a single thin slab with electron density ρ and thickness $d \ll \lambda$, the reflected and transmitted waves are functions of the incident wave

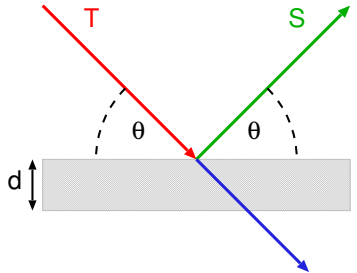

for large q, the reflected wave is weak with a phase shift of π

Darwin approach – single layer reflectivity

Consider a single thin slab with electron density ρ and thickness $d \ll \lambda$, the reflected and transmitted waves are functions of the incident wave

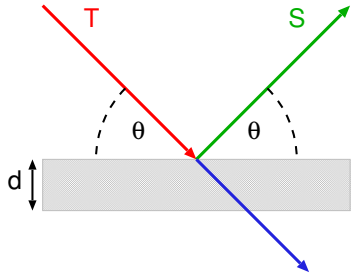

for large q, the reflected wave is weak with a phase shift of π

$$S = -igT$$

Darwin approach – single layer reflectivity

Consider a single thin slab with electron density ρ and thickness $d \ll \lambda$, the reflected and transmitted waves are functions of the incident wave

where

$$g = \frac{\lambda r_0 \rho d}{\sin\theta}$$

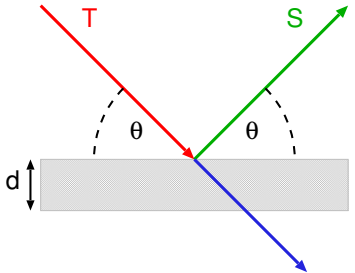

for large q, the reflected wave is weak with a phase shift of π

$$S = -igT$$

Darwin approach – single layer reflectivity

Consider a single thin slab with electron density ρ and thickness $d \ll \lambda$, the reflected and transmitted waves are functions of the incident wave

where $$g = \frac{\lambda r_0 \rho d}{\sin\theta}$$

if the layer is made up of unit cells with volume v_c and structure factor $F \xrightarrow{Q=0} Z$, the electron density is $\rho = |F|/v_c$ and using the Bragg condition, we can rewrite g as

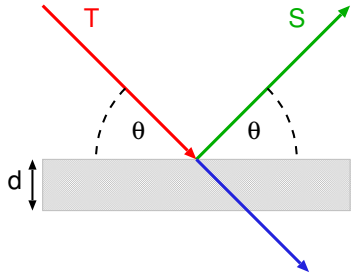

for large q, the reflected wave is weak with a phase shift of π

$$S = -igT$$

Darwin approach – single layer reflectivity

Consider a single thin slab with electron density ρ and thickness $d \ll \lambda$, the reflected and transmitted waves are functions of the incident wave

where $$g = \frac{\lambda r_0 \rho d}{\sin\theta}$$

if the layer is made up of unit cells with volume v_c and structure factor $F \xrightarrow{Q=0} Z$, the electron density is $\rho = |F|/v_c$ and using the Bragg condition, we can rewrite g as

$$g = \frac{[2d \sin\theta/m] r_0 (|F|/v_c) d}{\sin\theta}$$

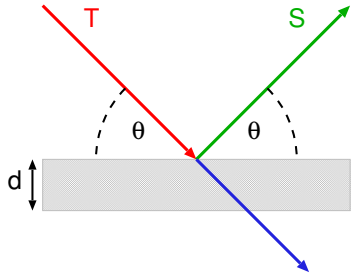

for large q, the reflected wave is weak with a phase shift of π

$$S = -igT$$

Darwin approach – single layer reflectivity

Consider a single thin slab with electron density ρ and thickness $d \ll \lambda$, the reflected and transmitted waves are functions of the incident wave

where $$g = \frac{\lambda r_0 \rho d}{\sin\theta}$$

if the layer is made up of unit cells with volume v_c and structure factor $F \xrightarrow{Q=0} Z$, the electron density is $\rho = |F|/v_c$ and using the Bragg condition, we can rewrite g as

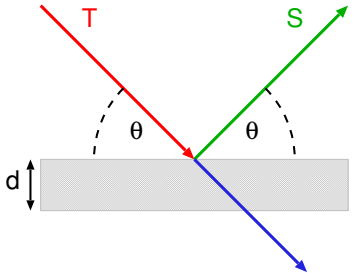

for large q, the reflected wave is weak with a phase shift of π

$$S = -igT$$

$$g = \frac{[2d\sin\theta/m]r_0(|F|/v_c)d}{\sin\theta} = \frac{1}{m}\frac{2d^2 r_0}{v_c}|F|$$

Darwin approach – single layer transmission

$$g = \frac{1}{m}\frac{2d^2 r_0}{v_c}|F| = \frac{\lambda r_0 d}{v_c \sin\theta}|F|$$

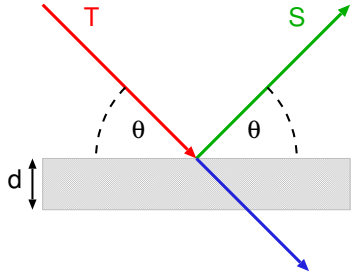

Darwin approach – single layer transmission

$$g = \frac{1}{m}\frac{2d^2 r_0}{v_c}|F| = \frac{\lambda r_0 d}{v_c \sin\theta}|F|$$

since $v_c \sim d^3$ then $g \sim r_0/d \approx 10^{-5}$

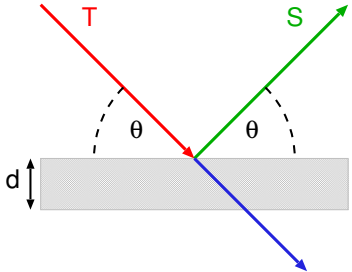

Darwin approach – single layer transmission

$$g = \frac{1}{m}\frac{2d^2 r_0}{v_c}|F| = \frac{\lambda r_0 d}{v_c \sin\theta}|F|$$

since $v_c \sim d^3$ then $g \sim r_0/d \approx 10^{-5}$

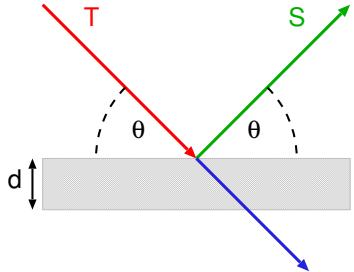

the transmitted wave is equal in amplitude to the incident wave but gains a phase shift as it passes through the layer

Darwin approach – single layer transmission

$$g = \frac{1}{m}\frac{2d^2 r_0}{v_c}|F| = \frac{\lambda r_0 d}{v_c \sin\theta}|F|$$

since $v_c \sim d^3$ then $g \sim r_0/d \approx 10^{-5}$

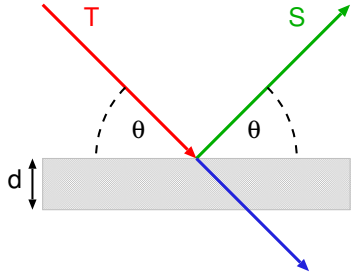

the transmitted wave is equal in amplitude to the incident wave but gains a phase shift as it passes through the layer

$$T' = (1 - ig_0)\,T$$

Darwin approach – single layer transmission

$$g = \frac{1}{m}\frac{2d^2 r_0}{v_c}|F| = \frac{\lambda r_0 d}{v_c \sin\theta}|F|$$

since $v_c \sim d^3$ then $g \sim r_0/d \approx 10^{-5}$

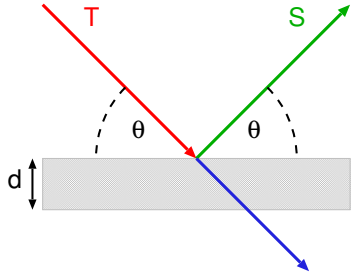

the transmitted wave is equal in amplitude to the incident wave but gains a phase shift as it passes through the layer

$$T' = (1 - ig_0)T \approx e^{-ig_0}T$$

Darwin approach – single layer transmission

$$g = \frac{1}{m}\frac{2d^2 r_0}{v_c}|F| = \frac{\lambda r_0 d}{v_c \sin\theta}|F|$$

since $v_c \sim d^3$ then $g \sim r_0/d \approx 10^{-5}$

from Chapter 3

$$g_0 = \frac{\lambda \rho_{at} f^0(0) r_0 d}{\sin\theta}$$

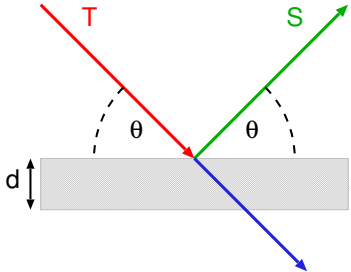

the transmitted wave is equal in amplitude to the incident wave but gains a phase shift as it passes through the layer

$$T' = (1 - ig_0)T \approx e^{-ig_0}T$$

Darwin approach – single layer transmission

$$g = \frac{1}{m}\frac{2d^2 r_0}{v_c}|F| = \frac{\lambda r_0 d}{v_c \sin\theta}|F|$$

since $v_c \sim d^3$ then $g \sim r_0/d \approx 10^{-5}$

from Chapter 3

$$g_0 = \frac{\lambda \rho_{at} f^0(0) r_0 d}{\sin\theta} = \frac{\lambda |F_0| r_0 d}{v_c \sin\theta}$$

where $|F_0| = \rho_{at} f^0(0) v_c$ is the unit cell structure factor in the forward direction at $Q = \theta = 0$

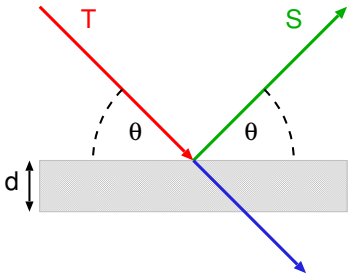

the transmitted wave is equal in amplitude to the incident wave but gains a phase shift as it passes through the layer

$$T' = (1 - ig_0)T \approx e^{-ig_0}T$$

Darwin approach – single layer transmission

$$g = \frac{1}{m}\frac{2d^2 r_0}{v_c}|F| = \frac{\lambda r_0 d}{v_c \sin\theta}|F|$$

since $v_c \sim d^3$ then $g \sim r_0/d \approx 10^{-5}$

from Chapter 3

$$g_0 = \frac{\lambda \rho_{at} f^0(0) r_0 d}{\sin\theta} = \frac{\lambda |F_0| r_0 d}{v_c \sin\theta}$$

where $|F_0| = \rho_{at} f^0(0) v_c$ is the unit cell structure factor in the forward direction at $Q = \theta = 0$

this can be rewritten in terms of g as

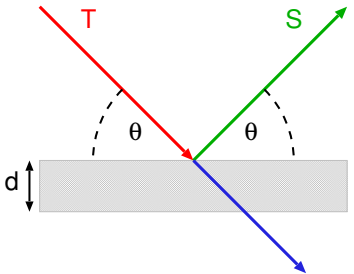

the transmitted wave is equal in amplitude to the incident wave but gains a phase shift as it passes through the layer

$$T' = (1 - ig_0)T \approx e^{-ig_0}T$$

Darwin approach – single layer transmission

$$g = \frac{1}{m}\frac{2d^2 r_0}{v_c}|F| = \frac{\lambda r_0 d}{v_c \sin\theta}|F|$$

since $v_c \sim d^3$ then $g \sim r_0/d \approx 10^{-5}$

from Chapter 3

$$g_0 = \frac{\lambda \rho_{at} f^0(0) r_0 d}{\sin\theta} = \frac{\lambda |F_0| r_0 d}{v_c \sin\theta}$$

where $|F_0| = \rho_{at} f^0(0) v_c$ is the unit cell structure factor in the forward direction at $Q = \theta = 0$

this can be rewritten in terms of g as

$$g_0 = g\frac{|F_0|}{|F|}$$

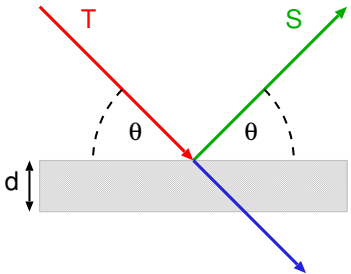

the transmitted wave is equal in amplitude to the incident wave but gains a phase shift as it passes through the layer

$$T' = (1 - ig_0)T \approx e^{-ig_0}T$$